Numerical Aspects of the Implementation of Artificial Boundary Conditions for Laminar Fluid-Structure Interactions

C. Boeckle[*1], and P. Wittwer[1]
[1] Dept. of Theoretical Physics, University of Geneva, Switzerland
*Corresponding author: 24, quai Ernest-Ansermet, CH-1211 Genève 4. christoph.boeckle@unige.ch

Abstract: We discuss the implementation of artificial boundary conditions for stationary Navier-Stokes flows past bodies in the half-plane, for a range of low Reynolds numbers. When truncating the half-plane to a finite domain for numerical purposes, artificial boundaries appear. We present an explicit Dirichlet condition for the velocity at these boundaries in terms of an asymptotic expansion for the solution to the problem. We show a substantial increase in accuracy of the computed values for drag and lift when compared with results for traditional boundary conditions. We also analyze the qualitative behavior of the solutions in terms of the streamlines of the flow.

Keywords: Navier-Stokes, exterior domain, fluid-structure interaction, computational fluid dynamics, artificial boundary conditions

1. Introduction

We numerically solve the Navier-Stokes equations for the flow past a body moving at constant velocity parallel to the boundary of a half-plane. We are particularly interested in the computation of the hydrodynamic forces acting on the body in the case where the body is small, and the flow is laminar.

Since we truncate the unbounded half-plane to finite sub-domains for the numerical treatment, the question of boundary conditions at the resulting artificial boundaries (a.b.) arises. We show that, when compared to traditional methods of "velocity-at-infinity" boundary conditions (see for example [1]) or "open" boundary conditions (see for example [2]), a significant gain in accuracy in the computed values of drag and lift can be obtained when using the asymptotic expansion for the velocity field constructed in [3] as Dirichlet boundary conditions.

We concentrate on drag and lift for the quantitative comparison of different boundary conditions because they are important quantities in engineering and theoretical work alike. Besides increased accuracy, the qualitative behavior of the flow within the computational domain is also improved with our boundary conditions in the sense that the streamlines are not significantly influenced by the artificial boundary, contrary to the cases where traditional boundary conditions are used.

Our aim is to describe the implementation of our adaptive boundary conditions and highlight the fundamental importance of the choice of boundary conditions when precision and qualitative correctness of the flow patterns are desired alongside a decrease in hardware requirements (especially in memory due to smaller computational domains).

Similar adaptive boundary conditions have been studied for the full plane, see [4] and [5], and the full space, see [6].

All mentions of COMSOL refer to COMSOL multiphysics version 3.5a, using the basic steady-state incompressible Navier-Stokes model in two dimensions.

1.1 Mathematical Description

We treat the problem as viewed from the moving body, of characteristic size $2r$ and at a distance d from the wall, so that we may numerically solve the stationary equation system

$$\boldsymbol{u} \cdot \nabla \boldsymbol{u} + \nabla p - \nu \Delta \mathbf{u} = 0\,, \qquad (1)$$

$$\nabla \cdot \boldsymbol{u} = 0\,, \qquad (2)$$

where $\boldsymbol{u}$ is the velocity field, p is the pressure and ν is the dynamic viscosity of the fluid. The boundary conditions on the wall, located at $y = 0$, are

$$\boldsymbol{u}|_{y=0} = \boldsymbol{u}_\infty\,, \qquad (3)$$

with $\boldsymbol{u}_\infty = (1,0)$ the opposite of the body velocity. The boundary conditions on the body may be chosen either as "slip" or "no slip", as defined in COMSOL. The conditions at the artificial boundaries are the object of the next section. For practical reasons, we only use domains of the form $D = \{(x,y)|-l \le x \le l, 0 \le y \le l\}$, where $l > d + r$. See **Figure 1** for a representation of the body and the domain.

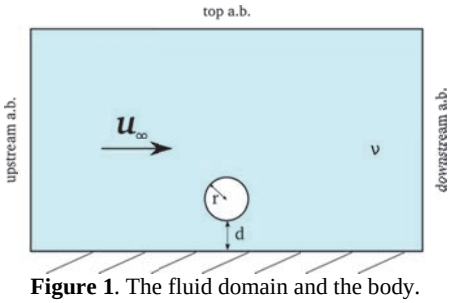

Figure 1. The fluid domain and the body.

Finally, for later use we define the viscous length scale and the Reynolds number

$$\ell_v = \frac{\nu}{u_\infty}, \qquad \mathrm{Re} = \frac{2\mathrm{r}}{\ell_v}. \tag{4}$$

2. Artificial Boundaries

Theoretically, the correct way to treat the edges of a domain which is obtained by a truncation of the half-plane would be to use the solution of the original problem in the half-plane evaluated along those edges as a Dirichlet boundary condition. Of course, the solution of the original problem is unknown. One must therefore find boundary conditions which represent a good approximation to the solution of the original problem. We define and investigate three choices: *simple* boundary conditions (s.b.c.), *classic* (or open) boundary conditions (c.b.c.) and *adaptive* boundary conditions (a.b.c.), *i.e.*, the new scheme which we propose here. More precisely:

• The s.b.c. prescribe $\boldsymbol{u}_\infty$ on all the a.b.

• The c.b.c. prescribe $\boldsymbol{u}_\infty$ on the upstream a.b. in order to fix the inflow, and the "normal stress" open boundary with $f_0 = 0$ on the remaining a.b., allowing in and outflow.

• The a.b.c. use expressions (5) and (6) which are based on the asymptotic expansion of the mathematical solution of the half-plane problem, to prescribe the velocity at the a.b.

The s.b.c., while a reasonable starting point, are nevertheless problematic, as they do not allow fluid to move through the artificial boundary parallel to the wall, making the problem effectively a channel flow. This impacts flow rate conservation in two problematic ways: first, the velocity of the fluid must increase artificially above and below the body, it cannot be adjusted thanks to fluid "exiting" through the top a.b.; second, the flow rate should in fact be lower in the truncated domain in comparison with the flow without a body, however the use of $\boldsymbol{u}_\infty$ at the upstream artificial boundary prescribes the same flow as without a body. See [1] for an example where such boundary conditions are used in the three-dimensional version of the problem considered here. A recent work using these boundary conditions, albeit for a flow in the full plane around two side-by-side cylinders, is [7], where the authors have run simulations in domains with sizes 750 by 500 cylinder radii to ensure that perturbations due to the boundary conditions are small enough.

The c.b.c. are mixed Dirichlet (pressure) and Neumann (velocity) boundary conditions. See [2] for a three-dimensional implementation of the problem considered here. While the c.b.c. are less restrictive on the flow rate than the s.b.c., the condition on the upstream a.b. still prescribes a flow rate which is too large.

We now present our adaptive boundary conditions, which prescribe the asymptotic expansion $\boldsymbol{u}_{\mathrm{as}} = (u_{as}, v_{as})$ to the velocity field at the artificial boundaries

$$\begin{aligned} u_{as} = u_\infty \Bigg(1 &+ \frac{c_1}{(y/\ell_v)^{3/2}} \varphi_1\left(\frac{x}{y}\right) \\ &+ \frac{c_1}{(y/\ell_v)^2} \varphi_2\left(\frac{x}{y}\right) \\ &+ \frac{c_1}{(y/\ell_v)^2} \eta_1\left(\frac{\ell_v x}{y^2}\right) \\ &+ \frac{c_1}{(y/\ell_v)^3} \eta_2\left(\frac{\ell_v x}{y^2}\right) \Bigg) \end{aligned} \tag{5}$$

$$\begin{aligned} v_{as} = u_\infty \Bigg(&\frac{c_1}{(y/\ell_v)^{3/2}} \psi_1\left(\frac{x}{y}\right) \\ &+ \frac{c_1}{(y/\ell_v)^2} \psi_2\left(\frac{x}{y}\right) \\ &+ \frac{c_1}{(y/\ell_v)^3} \omega_1\left(\frac{\ell_v x}{y^2}\right) \\ &+ \frac{c_1}{(y/\ell_v)^4} \omega_2\left(\frac{\ell_v x}{y^2}\right) \Bigg) \end{aligned} \tag{6}$$

See Appendix 7.1 for a description of the constituent functions.

The constant c_1 appearing in (5) and (6) is a real number depending on the flow and body parameters in a sophisticated manner. It can be computed during run-time thanks to the algorithm presented in Appendix 7.2.

For a rigorous mathematical derivation of this asymptotic expansion, see [8], [9] and [3]. For the adaptation to numerical application, see [10].

3. Results

The simulations presented in this section are performed with arbitrary meshes generated by COMSOL. The linear system is solved using the direct linear solver PARDISO, and the nonlinear solver is the damped Newton scheme. For all the simulations presented below, a workstation with 36 GB RAM and a 12-core processor was used.

All bodies presented in this section are circles with a radius $r = 0.5$, and have Slip boundary conditions. See [10] for more cases with different Reynolds numbers (0.005 to 25), both No slip and Slip boundary conditions on the body and various body shapes. Nevertheless, our presentation captures the essential features of the adaptive boundary conditions.

3.1 Qualitative behavior

In a first step, we show that the choice of boundary conditions has an important impact on the fluid flow.

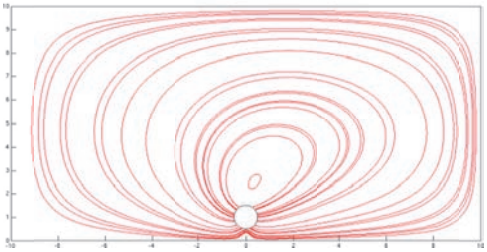

Figure 2. Streamlines of $\boldsymbol{u} - \boldsymbol{u}_\infty$, with s.b.c.

To showcase this, we represent in **Figures 2-4** the streamlines for the velocity field from which the constant flow $\boldsymbol{u}_\infty$ has been subtracted, on domains with $l = 10$. For the sake of brevity, we shall only consider the case with $\mathrm{Re} = 1$.

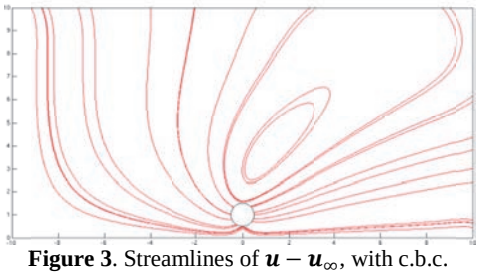

Figure 3. Streamlines of $\boldsymbol{u} - \boldsymbol{u}_\infty$, with c.b.c.

In the case of the s.b.c., see **Figure 2**, we observe an artificial backflow (moving clockwise on **Figure 2**). A very important proportion of the computational domain is thus used to compute this non-physical flow.

In the case of the c.b.c., see **Figure 3**, this backflow is not present, but the flow is still significantly influenced by the artificial boundaries, as can be seen by looking at the streamlines.

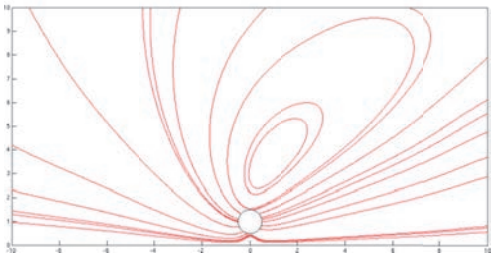

Figure 4. Streamlines of $\boldsymbol{u} - \boldsymbol{u}_\infty$, with a.b.c.

The a.b.c., see **Figure 4**, are the only ones that yield qualitatively satisfying flows all the way up to the boundary, and the streamlines exhibit almost no distortion near the boundary.

3.2 Quantitative examination of lift and drag

We present in **Figures 5 & 6** the drag and lift acting on our body at $\mathrm{Re} = 1$, computed thanks to COMSOL's native post-processing features.

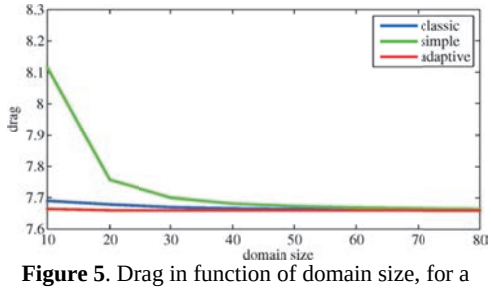

Figure 5. Drag in function of domain size, for a circular body with slip b.c., at $\mathrm{Re} = 1$.

As the simulations with adaptive a.b.c. present the least variation with domain size, we use the largest simulation ($l = 90$) feasible on our workstation using these boundary conditions as a reference for the computation of relative errors. The actual values are obtained thanks to a Richardson extrapolation scheme operating on four values obtained from successively refined simulations (each mesh element divided into four smaller ones).

Our reference values for drag and lift are:

$$\text{Re} = 0.5: \quad F_D = 14.497, F_L = 0.88013, \quad (7)$$

$$\text{Re} = 1: \quad F_D = 7.6597, F_L = 0.84732, \quad (8)$$

$$\text{Re} = 5: \quad F_D = 2.0916, F_L = 0.59219, \quad (9)$$

$$\text{Re} = 10: \quad F_D = 1.3014, F_L = 0.37568, \quad (10)$$

$$\text{Re} = 25: \quad F_D = 0.71307, F_L = 0.10162. \quad (11)$$

Figures 7 & 8 represent the relative error on drag and lift for a sequence of simulations with Reynolds numbers $\text{Re} = 0.5, 1, 5, 10, 25$.

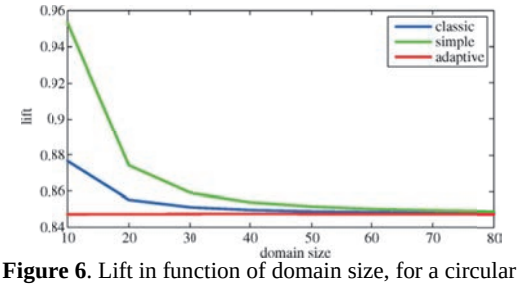

Figure 6. Lift in function of domain size, for a circular body with slip b.c., at $\text{Re} = 1$.

We observe that the s.b.c. overestimate the values of the forces compared to the c.b.c. which in turn overestimate the drag and lift compared to the a.b.c., except for the drag in the case Re = 0.5 on the smallest domain. This was to be expected, since both the s.b.c. and c.b.c. impose a flow rate only appropriate in *absence* of a body. In a bounded domain, this flow rate is higher than when there is a body, leading to an inevitable overestimation in the forces.

4. Conclusions

We have presented simulations of flow around bodies in a half-plane. We have shown that thanks to the adaptive boundary conditions, the dependence of the computed values for drag and lift on the size of the computational domain is drastically reduced, achieving accuracy better by one to two orders of magnitude when compared to simulations with simple or classic boundary conditions.

Therefore, with the a.b.c., a given accuracy can be obtained on much smaller domains, thus bringing down the hardware requirements (CFD on a laptop).

We have also shown a substantial qualitative improvement of the physical behavior of the flow, in the sense that the adaptive boundary conditions have a minimal influence on the streamlines, in particular close to the artificial boundaries.

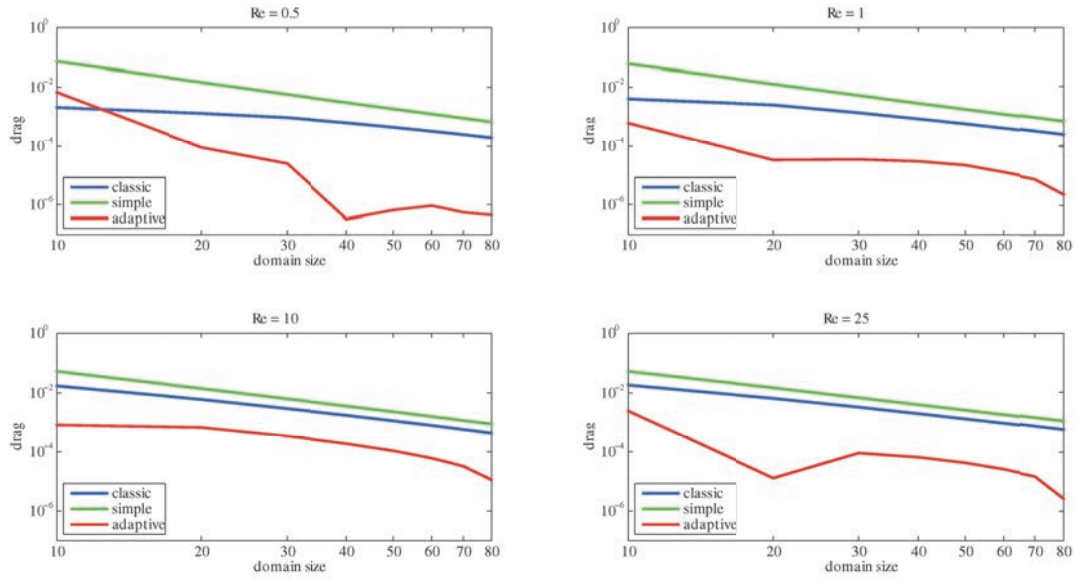

Figure 7. Relative error on drag in function of domain size, for a circular body with slip b.c., at $\text{Re} = 0.5, 1, 5, 10, 25$. Note the logarithmic scale.

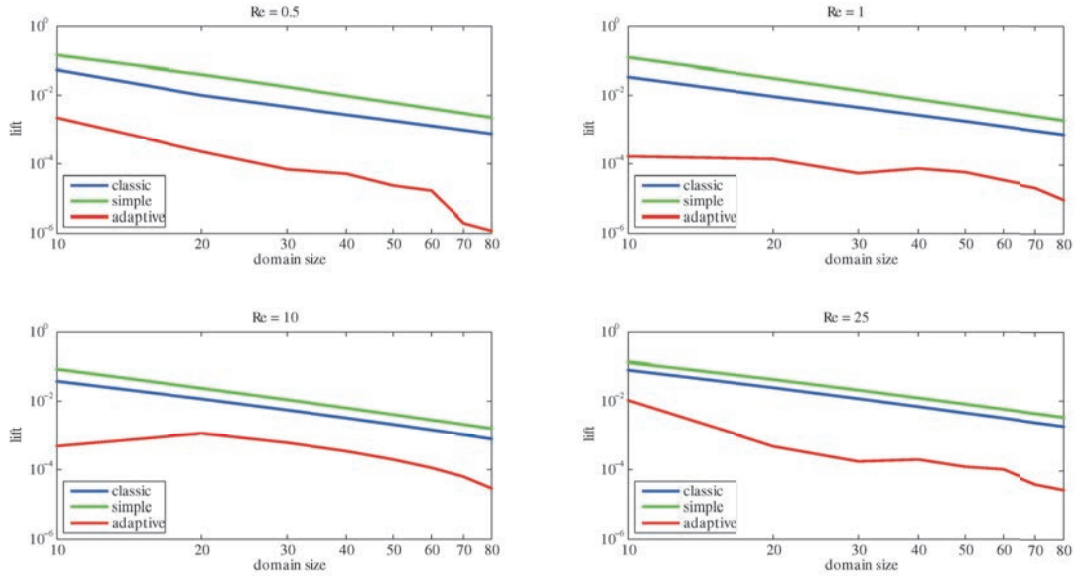

Figure 8. Relative error on lift in function of domain size, for a circular body with slip b.c., at Re $= 0.5, 1, 5, 10, 25$. Note the logarithmic scale.

5. References

1. L. Zeng, S. Balachandar and P. Fischer, Wall-induced forces on a rigid sphere at finite Reynolds number, *Journal of Fluid Mechanics*, **536**, 1-25 (2005)
2. B. Chen, T. Kawamura and Y. Kodama, Simulation of a single bubble rising along an inclination surface, *Proceedings of the 17th CFD Symposium*, Tokyo, Dec. 17th-19th, No. E8-3 (2003)
3. C. Boeckle and P. Wittwer, Asymptotics of solutions for a basic case of fluid-structure interaction, *arXiv.org*, 1109.1431 (2011) [submitted to *Nonlinear Analysis: Theory, Methods and Applications*]
4. D. Bichsel and P. Wittwer, Computation of Airfoils at Very Low Reynolds Numbers, *Proceedings of the COMSOL Users Conference*, Grenoble (2007)
5. S. Bönisch, V. Heuveline and P. Wittwer, Second order adaptive boundary conditions for exterior flow problems, *Journal of Mathematical Fluid Mechanics*, **10**, 45-70 (2008)
6. V. Heuveline and P. Wittwer, Adaptive boundary conditions for exterior stationary flows in three dimensions, *Journal of Mathematical Fluid Mechanics*, **12**, 554-575 (2010)
7. A. Vakil and S. I. Green, Two-dimensional side-by-side circular cylinders at moderate Reynolds numbers, *Computers & Fluids*, **51**, 136-144 (2011)
8. M. Hillairet and P. Wittwer, Existence of Stationary Solutions of the Navier-Stokes Equations in Two Dimensions in the Presence of a Wall, *Journal of Evolution Equations*, **9**, 675-706 (2009)
9. C. Boeckle and P. Wittwer, Decay Estimates for Solutions of the Two-Dimensional Navier-Stokes Equations in the Presence of a Wall, *SIAM Journal on Mathematical Analysis*, **in print**, (2012)
10. C. Boeckle and P. Wittwer, Artificial Boundary Conditions for Stationary Navier-Stokes Flows Past Bodies in the Half-Plane, *arXiv.org*, 1208.3648 (2012) [submitted to *Computers & Fluids*]

6. Acknowledgements

The authors are supported by the Swiss National Science Foundation (Grant No. 200021-124403).

7. Appendix

7.1 Special functions

We present the particular functions used in expressions (5) and (6). We have

$$\varphi_1(z) = -\frac{1}{4\sqrt{\pi}}\frac{r+1-z^2+zr+2z}{r^3\sqrt{r+1}} \quad (12)$$

$$\psi_1(z) = -\frac{1}{4\sqrt{\pi}}\frac{r+1-z^2-zr-2z}{r^3\sqrt{r+1}} \quad (13)$$

$$\varphi_2(z) = -\frac{2}{\pi}\frac{z}{r^4} \quad (14)$$

$$\psi_2(z) = -\frac{1}{\pi}\frac{1-\mathrm{z}^2}{r^4} \quad (15)$$

with

$$r = \sqrt{1+\mathrm{z}^2} \quad (16)$$

and

$$\eta_1(z) = \frac{1}{2\sqrt{\pi z^3}}\begin{cases} e^{-1/4z}, & z \geq 0 \\ 0, & z < 0 \end{cases} \quad (17)$$

$$\omega_1(z) = \frac{1-2z}{4\sqrt{\pi z^5}}\begin{cases} e^{-1/4z}, & z \geq 0 \\ 0, & z < 0 \end{cases} \quad (18)$$

$$\eta_2(z) = \frac{1}{4\pi z^3}\Big(2z + \sqrt{\pi|z|}(1 - 2z)e^{-\frac{1}{4z}}E(z)\Big) \quad (19)$$

$$\omega_2(z) = \frac{1}{8\pi z^4}\Big(2z(1-4z) + \sqrt{\pi|z|}(1 - 6z)e^{-\frac{1}{4z}}E(z)\Big) \quad (20)$$

with

$$E(z) = \begin{cases} -\mathrm{erfi}(1/2|z|), & z \geq 0 \\ \mathrm{erfc}(1/2|z|), & z < 0 \end{cases} \quad (21)$$

where

$$\mathrm{erfi}(z) = -i\,\mathrm{erf}(iz) \quad (22)$$

$$\mathrm{erfc}(z) = 1 - \mathrm{erf}(z) \quad (23)$$

with

$$\mathrm{erf}(z) = \frac{2}{\sqrt{\pi}}\int_0^z \mathrm{e}^{-t^2}dt \quad (24)$$

the error function and i the imaginary number.

All these functions were implemented using an interface to Matlab (tested on versions 2009a and 2010a). For the imaginary error function, erfi, we used a function by Per Sundqvist to be found on the Matlab Central website.

In the case of functions (19) and (20), numerical instability was an issue near $z = 0$, which was solved when using the respective Taylor expansions in that neighborhood

$$\eta_2^{(\mathrm{T})}(z) = -\frac{4}{\pi}(1 + 12z + 180z^2 + 3360z^3 + \cdots) \quad (25)$$

$$\omega_2^{(\mathrm{T})}(z) = -\frac{12}{\pi}(1 + 20z + 420z^2 + 10080z^3 + \cdots) \quad (26)$$

See [10] for additional details.

7.2 Algorithm for the determination of the special constant in the asymptotic expansion

The constant c_1 depends on the solution, see [10]. An algorithm to find a good approximation is presented here. In essence, it searches for the root of the function

$$g(x) = \frac{1}{n_1}\int_D \nabla\cdot(\mathrm{T}(\boldsymbol{u},p)\boldsymbol{V})\,dD - x \quad (27)$$

with D the fluid domain and

$$\mathrm{T} = -\boldsymbol{u}\otimes\boldsymbol{u} + \nu(\nabla\boldsymbol{u} + (\nabla\boldsymbol{u})^T) - p\mathbb{I} \quad (28)$$

calculated with $\boldsymbol{u}$ and p computed from the numerical solution obtained with the a.b.c. with c_1 such that $g(c_1) = 0$ and where $\otimes$ represents the dyadic product (*i.e.*, $(\boldsymbol{a}\otimes\boldsymbol{b})_{ij} = a_i b_j$) and

$$\boldsymbol{V} = (\sqrt{y}\chi_D(x,y), 0) \quad (29)$$

with $\chi_D(x,y) = \chi_x(x)\cdot\chi_y(y)$ any user-defined differentiable cut-off function that cuts a channel perpendicular to the wall centered on the body and two strips, one adjacent to the wall and one adjacent to the top artificial. The scalar n_1 in (27) is given by

$$\begin{aligned} n_1(\ell_v, l) &= \int_1^\infty \chi_y(l/z)\left(\ell_v^{3/2}\frac{\varphi_1(z)-\psi_1(z)}{z} + 2\ell_v^2\frac{\varphi_2(z)}{\sqrt{zl}}\right)dz \\ &- \int_{\ell_v/l}^\infty \chi_y\left(\sqrt{\ell_v l/z}\right)\left(\ell_v^2\frac{\eta_1(z)}{(\ell_v l z^3)^{1/4}} + \ell_v^3\frac{\eta_2(z)-\eta_2(-z)}{(\ell_v^3 l^3 z)^{1/4}}\right)dz \end{aligned} \quad (30)$$

and may be calculated ahead of time.

The first term in (27) is directly programmed in COMSOL as a subdomain expression. The cutoff expressions are programmed as global expressions. We chose

$$\chi_x(x) = \chi\left(-\frac{x+1}{4}\right)\cdot\chi\left(\frac{x-1}{4}\right) \quad (31)$$

$$\chi_y(y) = \chi\left(\frac{y}{4}\right)\cdot\chi\left(\frac{l-y}{4}\right) \quad (32)$$

where

$$\chi(z) = \int_0^{\max(0,\min(1,z))} h(z')dz' \quad (33)$$

$$h(z) = 630z^4(1-z)^4,\ 0 \leq z \leq 1 \quad (34)$$

Our root-finding algorithm operates from Matlab using the output of successive COMSOL simulations restarted from the last one (the first one uses $c_1 = 0$ and is thus equivalent to a simulation with s.b.c.)